

# On the global stability of rotating magnetized disks

L.L. Kitchatinov and M.V. Mazur

Institute for Solar-Terrestrial Physics, P.O. Box 4026, Irkutsk, 664033, Russia (kit@sitmis.irkutsk.su)

Received 24 July 1996 / Accepted 14 January 1997

**Abstract.** Global modes of the magnetic shear instability in horizontally unbounded rotating disks are studied by solving the linear eigenvalue problem. Nonaxisymmetry and finite diffusivities are allowed for. The instability exists in a range of the magnetic field amplitudes between the minimum value,  $B_{\min}$ , imposed by the finite diffusivities and the maximum amplitude,  $B_{\max}$ , brought about by the finite thickness of the disk. The unstable modes for the magnetic field close to the lower and upper bounds occupy different regions in the disk. The critical rotation rates for onset of the instability for the excitations with various axial and vertical symmetries are estimated and their dependencies on the external magnetic field amplitude are defined. The axisymmetric modes with symmetric magnetic field and antisymmetric velocity relative to the disk mid-plane are most easily excited. The effective diffusivity produced by the supernova explosions is small enough for the instability to be active in the galactic disk. The possibility of the *global* hydromagnetic dynamos excited by the instability in astrophysical disks is discussed.

**Key words:** instabilities – MHD – accretion disks – galaxies: magnetic fields

---

## 1. Motivation

The magnetic shear instability (Velikhov 1959; Chandrasekhar 1960) has recently become a subject of increasing astrophysical interest after Balbus & Hawley (1991) had noticed that the instability may provide a solution for the long-standing problem of the accretion disks turbulence origin. The hydrodynamically stable Keplerian disks are destabilized by a weak external magnetic field. The resulting small-scale turbulence may account for the effective viscosity ensuring the angular momentum outflow. The paper by Balbus & Hawley (1991) initiated many other works aimed mainly to understand the “microscopy”, i.e. the local properties, of the magnetic shear instability. The instability was found to be fast with the growth rates of the order of rotation frequency (Balbus & Hawley 1992). It indeed produces turbulence in nonlinear regime (Stone & Norman 1994; Brandenburg et al. 1995; Hawley et al. 1995; Matsumoto & Tajima 1995). Its astrophysical importance is not limited to the

accretion disks, but the instability may be relevant to the stellar spin-down physics ensuring rigid rotation in the radiative cores of the rotationally-braking stars (Balbus & Hawley 1994; Balbus 1995).

The magnetic shear instability may be equally relevant to “macroscopy” of the unstable bodies. The accretion disk turbulence is believed to produce global magnetic fields by the mean-field hydromagnetic dynamo mechanism (Deinzer et al. 1993; Rüdiger et al. 1995). Is the magnetic shear instability able to do so? A positive answer to this question would mean a completely new dynamo. Indeed, hydromagnetic dynamos are believed to require “sufficiently complicated” velocity fields (Moffatt 1978; Krause & Rädler 1980). After Cowling’s (1934) theorem, the differential rotation is “too simple” to produce any dynamo. The theorem covers, however, only the kinematic case of dynamically insignificant magnetic fields. A field of finite amplitude may, in principle, be amplified by sufficiently complicated 3D motions resulting from destabilization of the differential rotation by the global magnetic field *itself*. Such a nonlinear dynamo-instability, if exists, would link the macroscopy to microscopy supplying the large-scale magnetic field driving the small-scale shear instability.

Brandenburg et al. (1995, 1996) and Stone et al. (1996) found the small-scale dynamo by the magnetic shear instability which was also envisaged by Tout & Pringle (1992). The finding, however, does not mean the existence of the global dynamo. E.g., a (forced) mirror-symmetric turbulence is well known to produce the small-scale dynamos (cf. Pouquet et al. 1976; Meneguzzi et al. 1981) while the same turbulence can not generate the large-scale fields. Hence, the question of whether the global dynamos by the magnetic shear instability are possible seems to be open. An old recipe to answer the question is the development of a nonlinear global model. However, the entire spectrum of the spatial scales of the instability is hardly possible to resolve by such a model. The usual strategy is to describe explicitly the scales from the largest available to as small as possible and parameterize the still smaller scales by the effective diffusivities (Glatzmaier 1985; Glatzmaier & Roberts 1995).

It seems also not wise to attack the nonlinear problem from the very beginning. The linear global modes should be studied to get a guidance on where in the parametric space the global dynamo should be looked for.

The present paper considers the global modes of the magnetic shear instability in disk geometry. Recent global studies demonstrated the importance of boundaries imposed in vertical (Gammie & Balbus 1994) or horizontal (Curry et al. 1994; Curry & Pudritz 1995) directions. Our formulation is global over all dimensions and it includes the finite diffusivities (viscosity and resistivity). We neglect, however, compressibility and stratification which are, probably, not important for the shear instability proceeding via torsional noncompressive excitations. Note also that the finite diffusivities are not necessarily due to the unresolved small scales. They may be actual diffusivities of cool (protoplanetary) disks or may result from some other source of turbulence like supernova explosions in the galactic disk.

## 2. The model

### 2.1. The reference state

We consider a rotating disk of conducting fluid bounded by parallel plains normal to the rotation axis. The rotation is not uniform with the angular velocity dependent on the distance,  $s$ , to the rotation axis. The Brandt function is accepted for the angular velocity profile,

$$\Omega(s) = \Omega_0 f(s), \quad f(s) = \frac{1}{\left(1 + \left(\frac{s}{s_0}\right)^{nq}\right)^{\frac{1}{n}}}. \quad (1)$$

The profile tends to the value of  $\Omega_0$  at  $s \ll s_0$  and approaches the power law,  $\Omega \simeq \Omega_0 (s_0/s)^q$ , for large axial distances,  $s \gg s_0$ .

A uniform external magnetic field,  $\mathbf{B}_0$ , is imposed in vertical direction. Finite diffusivities of this model do not allow a steady reference state with any other external field pattern.

No boundaries over horizontal directions are imposed.

### 2.2. Outline of the mathematical formulation

Our equation system includes the induction equation,

$$\frac{\partial \mathbf{B}}{\partial t} = \text{rot}(\mathbf{V} \times \mathbf{B}) + \eta \Delta \mathbf{B}, \quad (2)$$

and a very similar looking vorticity equation,

$$\frac{\partial \mathcal{W}}{\partial t} = \text{rot}(\mathbf{V} \times \mathcal{W}) + \text{rot}(\mathbf{J} \times \mathbf{B})/c\rho + \nu \Delta \mathcal{W}, \quad (3)$$

where  $\mathcal{W} = \text{rot} \mathbf{V}$  is the vorticity,  $\mathbf{J} = c \text{rot} \mathbf{B}/4\pi$  is the current density,  $\nu$  is the viscosity, and  $\eta$  is the magnetic diffusivity. Eq. (3) results from curling the motion equation to exclude pressure.

Next, the dimensionless variables are introduced:

$$t = \frac{H^2}{\eta} t', \quad \mathbf{r} = H \mathbf{x}, \quad \mathbf{B} = B_0 \mathbf{b},$$

$$\mathbf{V} = H \Omega_0 \mathbf{v}, \quad \mathcal{W} = \Omega_0 \boldsymbol{\omega}, \quad \mathbf{J} = \frac{c B_0}{4\pi H} \mathbf{j}, \quad (4)$$

where  $H$  is the half-thickness of the disk, capital and small letters signify dimensional and normalized variables respectively. We linearize Eqs. (2) and (3) about the reference state of the preceding section to find

$$\begin{aligned} \frac{\partial \mathbf{b}}{\partial t} &= C_\Omega \text{rot}(s f(s) \mathbf{e}_\phi \times \mathbf{b} + \mathbf{v} \times \mathbf{e}) + \Delta \mathbf{b}, \\ \frac{\partial \boldsymbol{\omega}}{\partial t} &= C_\Omega \text{rot}\left(s f(s) \mathbf{e}_\phi \times \boldsymbol{\omega} + \frac{\hat{\kappa}^2}{2f(s)} \mathbf{v} \times \mathbf{e}\right) \\ &\quad + \frac{\text{Pm Ha}^2}{C_\Omega} \text{rot}(\mathbf{j} \times \mathbf{e}) + \text{Pm} \Delta \boldsymbol{\omega}, \end{aligned} \quad (5)$$

where  $\hat{\kappa}$  is the normalized epicyclic frequency,

$$\hat{\kappa}^2 = \frac{2f}{s} \frac{d(s^2 f)}{ds} = 2f^2(s)(2 + \beta), \quad (6)$$

$\beta$  is the normalized shear,

$$\beta = \frac{s}{f(s)} \frac{df(s)}{ds} = -\frac{q(s/s_0)^{nq}}{1 + (s/s_0)^{nq}}, \quad (7)$$

$\mathbf{e} = \boldsymbol{\Omega}/\Omega$  and  $\mathbf{e}_\phi$  are the vertical and the azimuthal unit vectors respectively. Three dimensionless parameters of the Eqs. (5),

$$C_\Omega = \frac{\Omega_0 H^2}{\eta}, \quad \text{Ha} = \frac{B_0 H}{\sqrt{4\pi\rho\nu\eta}}, \quad \text{Pm} = \frac{\nu}{\eta}, \quad (8)$$

are the  $C_\Omega$  of the dynamo models, the Hartmann number, and the magnetic Prandtl number respectively.

All the vector fields in (5) are divergence-free and can be expressed in terms of scalar potentials defining their toroidal and poloidal parts:

$$\begin{aligned} \mathbf{v} &= \mathbf{e} \times \nabla U + \text{rot}(\mathbf{e} \times \nabla \Psi), \\ \mathbf{b} &= \mathbf{e} \times \nabla \mathcal{B} + \text{rot}(\mathbf{e} \times \nabla A). \end{aligned} \quad (9)$$

Similar representations for vorticity and current density,

$$\begin{aligned} \boldsymbol{\omega} &= \mathbf{e} \times \nabla W + \text{rot}(\mathbf{e} \times \nabla U), \\ \mathbf{j} &= \mathbf{e} \times \nabla \mathcal{J} + \text{rot}(\mathbf{e} \times \nabla \mathcal{B}), \end{aligned} \quad (10)$$

include two potentials identical with that from (9), while two other potentials obey the steady differential equations:

$$\begin{aligned} \hat{R}(\mathcal{J} + \Delta A) &= 0, \\ \hat{R}(W + \Delta \Psi) &= 0, \end{aligned} \quad (11)$$

where  $\hat{R}$  is the ‘‘horizontal part’’ of the Laplacian,

$$\hat{R} = \frac{1}{s} \frac{\partial}{\partial s} s \frac{\partial}{\partial s} + \frac{1}{s^2} \frac{\partial^2}{\partial \phi^2}. \quad (12)$$

The representations (9) and (10) are very similar to that used in spherical geometry (Chandrasekhar 1961, p.622). Also the derivation procedure of the dynamical equations for the potential functions is quite parallel to their derivation for spheres (cf. Krause & Rädler 1980; Moss et al. 1991). We substitute (9)

and (10) into (5) and take the scalar product of the resulting equations with the vertical unit vector  $e$ . It yields the dynamical equations for  $(\hat{R}A)$  and  $(\hat{R}U)$ . Next, the scalar product of  $e$  with curled Eqs. (5) give the dynamical equations for  $(\hat{R}\mathcal{B})$  and  $(\hat{R}W)$ . The equation system is too bulky to reproduce here. The final equations for the global modes are given in the Appendix A.

The boundary conditions for the flow require the vertical velocity to vanish and the boundaries to be stress-free:

$$\Psi = 0, \quad W = 0, \quad \frac{\partial U}{\partial z} = 0 \quad \text{at } z = \pm 1. \quad (13)$$

The ‘‘quasi-vacuum’’ boundary conditions for the magnetic field were applied,

$$\mathcal{B} = 0, \quad \frac{\partial A}{\partial z} = 0 \quad \text{at } z = \pm 1. \quad (14)$$

The conditions mean that the toroidal field is zero (as for the real vacuum) and poloidal field-lines are vertical on the boundaries. This later condition is definitely a weak point of our model. However, using the real (nonlocal) vacuum condition for the poloidal field makes the analysis of the horizontally-infinite disk unbearably complicated. We replace it by the quasi-vacuum condition with hope that the change does not produce any strong effect, which is normally the case.

The Fourier-expansions over  $z$  which automatically satisfy the conditions (13) and (14) are convenient:

$$\begin{aligned} \mathcal{B} = & \sum_{l=1}^{\infty} \mathcal{B}_l^c(s, \phi, t) \cos(\pi(l-1/2)z) \\ & + \sum_{n=1}^{\infty} \mathcal{B}_l^s(s, \phi, t) \sin(\pi lz), \end{aligned} \quad (15)$$

and the same for the potentials  $\Psi$  and  $W$ . Similarly,

$$\begin{aligned} A = & \sum_{l=1}^{\infty} A_l^s(s, \phi, t) \sin(\pi(l-1/2)z) \\ & + \sum_{l=1}^{\infty} A_l^c(s, \phi, t) \cos(\pi lz), \end{aligned} \quad (16)$$

and the same for  $\mathcal{J}$  and  $U$ . The first and the second sums in (15) and (16) describe the excitations with different types of symmetry relative to the mirror-reflection about the disk mid-plane. The first sums represent the symmetric magnetic field and the antisymmetric flow. The second ones - the antisymmetric magnetic field and the symmetric velocity. We shall use the notations S (symmetric) and A (antisymmetric) for these two types of excitations respectively. The complete equation system splits in two independent subsystems governing the S- and A-modes. Note again that the notations refer to the symmetry of magnetic field only, so that the S-modes combine the symmetric magnetic field with the antisymmetric flow, and v.v. for the A-modes.

A drastic simplification comes from the observation that the equations for different vertical wave-numbers,  $l$ , decouple

from each other (see Appendix A). Also the dependencies on the azimuth,  $\phi$ , decouple from the dependencies on the other coordinates. We write  $\mathcal{B}_l^s(s, \phi, t) = e^{im\phi} \mathcal{B}_{l,m}^s(s, t)$ , and the same for other potentials, to fix the azimuthal wave number of the modes. Consequently, the vertical,  $l$ , and the azimuthal,  $m$ , wave numbers should be included in the modes notations which now become S1,m and A1,m. E.g., S1,0 means the axisymmetric mode of symmetric magnetic field and antisymmetric velocity about the disc mid-plane with the vertical wave-number  $l = 1$ , A2,1 means the antisymmetric magnetic field and symmetric flow about the mid-plane with  $m = 1$  and  $l = 2$ , and so on.

The conditions on the rotation axis depend on the type of the axial symmetry. For the axisymmetric case, the horizontal components of the magnetic field and velocity should vanish at  $s = 0$  while the vertical components can be finite. For the modes with finite  $m$ , the vertical components should be zero at  $s = 0$ . In terms of the scalar potentials, the conditions read

$$\begin{aligned} \left( \frac{dA_l}{ds} \right)_{s=0} &= 0 \quad \text{for } m = 0, \\ (A_l)_{s=0} &= 0 \quad \text{for } m \neq 0, \end{aligned} \quad (17)$$

and the same for all other potentials.

The conditions for  $s \rightarrow \infty$  require that the excitations fall to zero at the very large distances.

As usual, assumption of the exponential time-dependencies,  $A, \mathcal{B}, \mathcal{J}, U, W, \Psi \sim e^{\sigma t}$ , reduces the linear stability analysis to the eigenvalue problem. The solutions were found numerically. The difficulty with the infinite range of variation of the axial distance,  $s$ , was resolved by a change to the new variable,

$$y = \frac{s/s_0}{1 + s/s_0}, \quad 0 \leq y \leq 1. \quad (18)$$

where  $s_0$  is the length-scale of the angular velocity variations (1). The uniform grid over  $y$  was applied which, of course, means a non-uniform grid over  $s$ . The eigenvalues and eigenvectors were identified by the inverse iteration procedure. The equation system used in the computations is given in the Appendix A.

### 3. Results and discussion

Apart from three basic governing parameters of Eq. (8), our model includes the parameters,  $n$  and  $q$ , of the rotation law (1), the aspect ratio,  $\alpha = s_0/H$ , and also the azimuthal,  $m$ , and the vertical,  $l$ , wave numbers. In order not to loose our way in the parametric space, we fix the values of those parameters, whose variations do not produce any qualitative changes in the results, to be constant:  $n = 2$ ,  $\text{Pm} = 1$ ,  $\alpha = 5$ .

Three values of the  $q$ -parameter of the rotation law (1) were considered, namely,  $q = 1$  implying constant azimuthal velocity at large axial distances which is usually assumed to be the case with galaxies,  $q = 1.5$  of the Keplerian rotation, and  $q = 2$  as the physically important case of marginal hydrodynamical stability.

Fig. 1 shows the neutral stability lines for the axisymmetric S1,0-modes on the  $C_\Omega$ -Ha plane for the three basic rotation

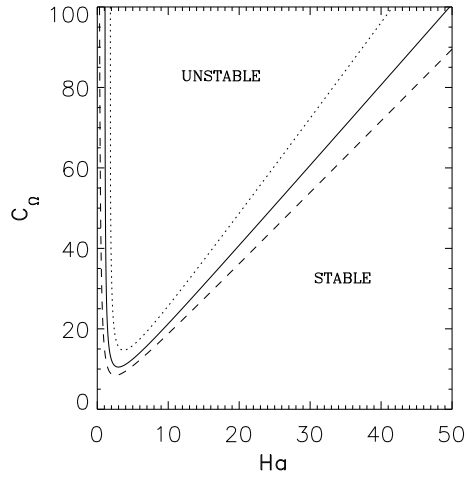


**Fig. 1.** The neutral stability lines for the axisymmetric S1,0-modes. The cases of Keplerian rotation with  $q = 1.5$  (full line), constant linear velocity,  $q = 1$  (dotted), and the marginally stable shear by the Rayleigh criterion,  $q = 2$  (dashed), are presented

laws. Remember that  $C_\Omega$  and  $Ha$  are the normalized rotation rate and the external magnetic field (8) respectively.

The critical rotation rates for onset of the instability in disks are much smaller compared to that for the spherical bodies (Kitchatinov & Rüdiger 1997). This is probably because of the diffusion over large horizontal scales of the disks is much less efficient. The disks become unstable roughly at  $C_\Omega \gtrsim 10$  provided that the external magnetic field amplitude assumes an appropriate value.

For not too slow rotation, there is a finite interval of the magnetic field amplitudes,  $B_{\min} < B < B_{\max}$ , where the system is unstable. The upper,  $B_{\min}$ , and lower,  $B_{\max}$ , bounds are imposed by the finite diffusivities and finite size of the system respectively (Balbus & Hawley 1991; Kitchatinov & Rüdiger 1997). The left branches of the neutral stability lines of Fig. 1 approach constant values of the Hartmann number for rapid rotation. This value is zero for the marginal shear,  $q = 2$ , of the Rayleigh stability criterion. Still, for any finite rotation rate a small but finite magnetic field is necessary to destabilise the disk with non-zero diffusivities. For any  $q$  larger than 2, the neutral stability lines cross the  $C_\Omega$ -axis indicating the non-magnetic instability. An example of such a behaviour is given on Fig. 2. Note that the destabilising effect by a weak magnetic field is still observable with the hydrodynamically supercritical shear: when the magnetic field is imposed, the instability onsets at smaller  $C_\Omega$  compared to the nonmagnetic threshold value of  $C_\Omega \simeq 66$ . This is because of  $q = 2.1$  is only slightly supercritical (cf. Appendix B).

Figs. 3 and 4 show that the excitations for the lower,  $B_{\min}$ , and upper,  $B_{\max}$ , bounds of the instability region occupy substantially different regions in the disk. The eigenmodes on the left branch of a neutral stability line settle on relatively large axial distances. Such a behaviour can be interpreted from the local stability analysis of the Appendix B.

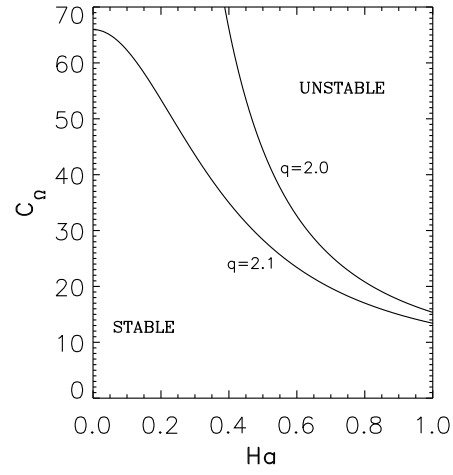


**Fig. 2.** Fragment of the stability diagrams for the marginal shear,  $q = 2$ , of the Rayleigh stability criterion and for the slightly supercritical value of  $q = 2.1$ . For the later case, the nonmagnetic instability is present at  $C_\Omega > 65.9$

For the marginally stable modes, we put the growth rate,  $\sigma$ , in Eq. (B4) to be equal zero which yields

$$\eta^2 k^4 = -\Omega^2(2 + \beta) - \omega_A^2 + \Omega [\Omega^2(2 + \beta)^2 + 4\omega_A^2]^{1/2}, \quad (19)$$

where  $k$  is the vertical wave number assuming discrete values in the disk of limited thickness,

$$\begin{aligned} k &= \pi(l - 1/2)/H && \text{for S - modes,} \\ k &= \pi l/H && \text{for A - modes,} \end{aligned} \quad (20)$$

$\omega_A$  is the Alfvén frequency for the external magnetic field, and  $\beta$  is the normalized shear (7). Consider first the lower bound,  $B_{\min}$ , of the instability region. Assuming the Alfvén frequency to be small compared to the rotation frequency, and  $\beta > -2$ , Eq. (19) gives

$$\frac{B_{\min}^2}{4\pi\rho} = \frac{\eta^2 k^2}{\frac{2}{|2+\beta|} - 1}. \quad (21)$$

Hence, the smaller (the larger in the absolute value) is shear,  $\beta$ , the smaller is the magnetic field producing the instability. The local shear (7) in our model decreases with distance,  $s$ . No surprise that the instability survives only at relatively large distances with minimum shear (Fig. 3) when magnetic field approaches  $B_{\min}$ . The distances, of course, should not be too large to ensure that the rotation rate (1) is larger than the Alfvén frequency.

The upper bound,  $B_{\max}$ , is imposed by the finite thickness of the disk, the diffusivities are of no significance there. Hence, we can neglect the left side of (19) when estimating  $B_{\max}$ . It yields,

$$\frac{B_{\max}^2 k^2}{4\pi\rho} = -2\beta\Omega^2. \quad (22)$$

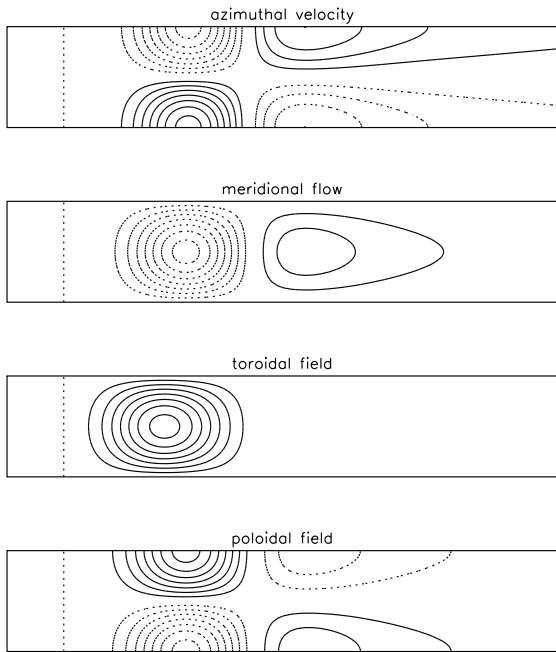


**Fig. 3.** S1,0-eigenmode in a Keplerian disk ( $q = -1.5$ ) for the left branch of the neutral stability line of Fig. 1 at  $C_\Omega = 70$ . From top to bottom: contour lines of the azimuthal velocity excitations,  $v_\phi$ , stream lines of the meridional flow, isolines of the toroidal magnetic field, and the lines of the poloidal magnetic field excitations. The full lines show positive levels and the clockwise circulation, and v.v. for the broken lines. The vertical and horizontal sizes are shown not in their actual proportion. The vertical dotted line indicates the distance  $s_0$

The right side of this equation is the product of  $-\beta(7)$ , which is steadily increasing function of  $s$ , with the steadily decreasing  $\Omega^2(1)$ . The product,  $-\beta\Omega^2$ , comes trough a maximum at distances of the order of  $s_0$ . This is, probably, why the instability survives only around the distance  $s_0$  when the field strength approaches  $B_{\max}$  (Fig. 4).

It seems natural to expect that the magnetic field in the excitations is mainly azimuthal because the dominating flow is the differential rotation. Figs. 5 and 6 show that the expectation comes true only for a weak external magnetic field. Close to  $B_{\max}$  the horizontal field is predominantly radial.

Until now we discussed only the S-modes with the smallest wave numbers. This is mainly because of these modes are excited most easily. The stability diagram for the A-modes is shown on Fig. 7. The antisymmetric excitations become unstable at considerably larger rotation rates compared to the S-modes (cf. Fig. 1). Also a larger vertical wave number,  $l$ , or a finite azimuthal wave number,  $m$ , lead to an increase in critical  $C_\Omega$ -values. Compare the minimum rotation rates,  $C_\Omega = 84.4$  and  $C_\Omega = 117$ , for the excitation of S2,0 and S1,1 modes respectively (for  $q = 1.5$ ) with the value of  $C_\Omega = 10.5$  for the S1,0-mode. The minimum magnetic field,  $B_{\min}$ , producing the instability is also increasing with the vertical wave number,  $l$ , in agreement with the estimation (21). Hence, the instability

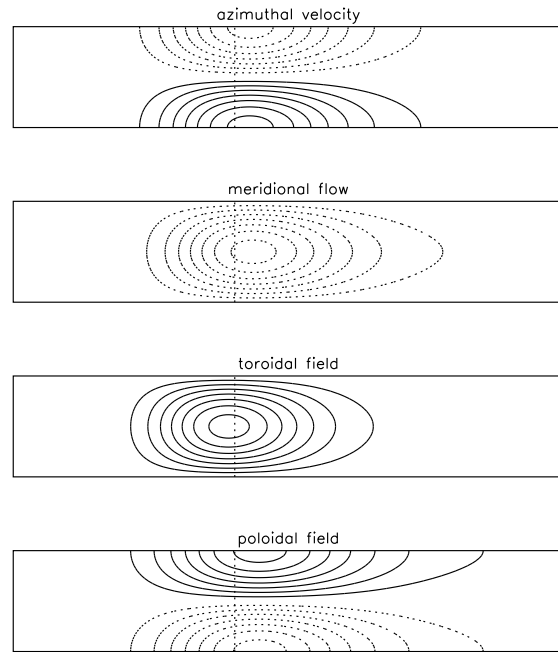


**Fig. 4.** The same as Fig. 3 but for the right branch of the neutral stability line. Note that the interval of axial distances for this figure is much smaller than that of Fig. 3

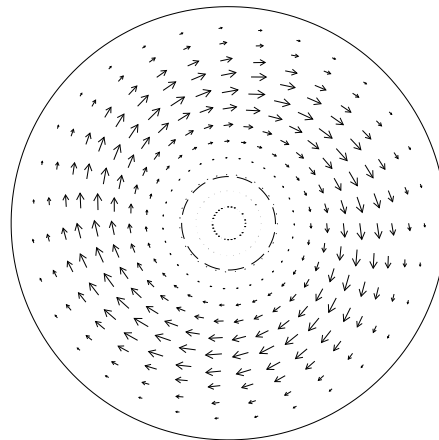


**Fig. 5.** Vector diagram of the magnetic field in the mid-plane of the disk for the marginally stable mode of Fig. 3 at the minimum external magnetic field producing the instability. The broken circle shows the distance  $s_0$

onsets on the *largest* available scale when the magnetic field is close to  $B_{\min}$ .

All the unstable axisymmetric excitations are steady, i.e., the imaginary parts of their eigenvalues equal zero. The nonaxisymmetric modes are oscillatory simply because of the co-rotation of the periodic in  $\phi$  excitations with the fluid relative to our inertial reference frame. The radial scales of the nonaxisymmetric modes are considerably smaller compared to the case of  $m = 0$ . This is, probably, due to the shearing effect by the differential rotation. The reduction of the horizontal scales ex-

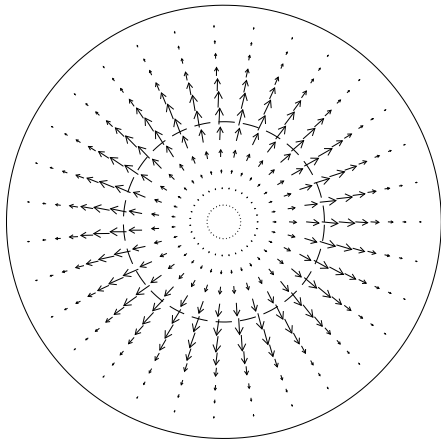


**Fig. 6.** Vector diagram of magnetic field in the mid-plane of the disk for the marginally stable mode of Fig. 4 at the maximum external magnetic field producing the instability. The broken circle shows the distance  $s_0$

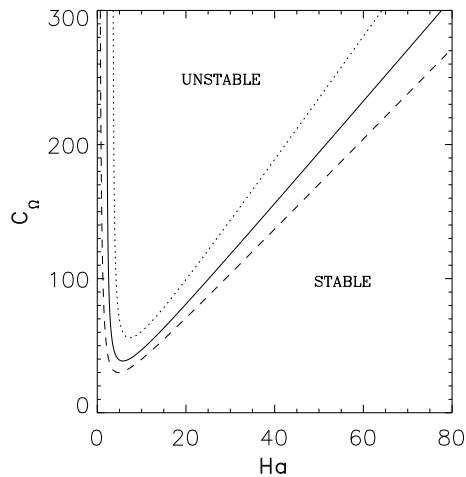


**Fig. 7.** The neutral stability lines for the axisymmetric A1,0-modes. The cases of Keplerian rotation with  $q = 1.5$  (full line), constant linear velocity,  $q = 1$  (dotted), and marginal hydrodynamical stability,  $q = 2$  (dashed), are presented

plain the excitation of these modes at larger  $C_\Omega$  compared to the axisymmetric case. The eigenvalues spectrum of the nonaxisymmetric modes is rather dense, though discrete. Fig. 8 shows the neutral stability lines for six nonaxisymmetric eigenmodes. Different modes are preferred in excitation in different regions on the  $C_\Omega$ -Ha plane. The eigenfrequencies of the neutrally stable modes increase from left to right lines of Fig. 8 indicating the locations of the eigenmodes for the later lines at relatively small axial distances with faster rotation. This picture indicates a preferential excitation of the nonaxisymmetric modes located at smaller  $s$  for stronger magnetic fields.

A deviation from axial symmetry is necessary for the hypothesized global dynamo. Therefore, the critical  $C_\Omega$  for the

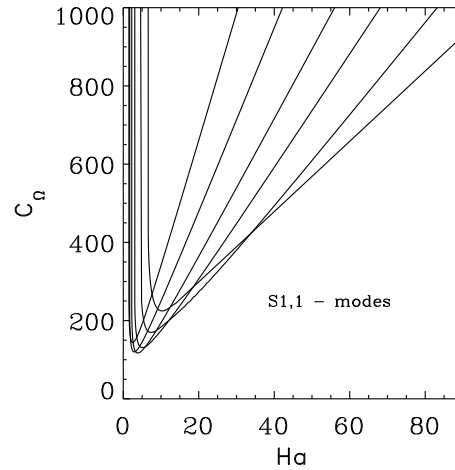


**Fig. 8.** Neutral stability lines for several S1,1 modes. Different modes have the smallest  $C_\Omega$  for the excitation for different Ha-values.  $q = 1.5$

dynamo may be expected to be of the order of some hundreds. In contrast to the global modes in spherical geometry (Kitchatinov & Rüdiger 1997), we did not find for the disks any region on the parametric plane where the excitation of nonaxisymmetric modes is preferred. This observation is unfavourable for the global dynamos. It may be noticed in this context, however, that *only* nonaxisymmetric modes are unstable with the toroidal background fields (Ogilvie & Pringle 1996).

Rather low critical  $C_\Omega$ -values for the onset of the magnetic shear instability in disks make it possible that the instability is active in galaxies. The supernova explosions produce a background effective diffusivities there. Kaisig et al. (1993) found  $\eta_{\text{expl}} \simeq 5 \cdot 10^{24} \text{ cm}^2 \text{ s}^{-1}$  for the explosions. Combining this value with the rotation rate of  $\Omega_0 \simeq 5 \cdot 10^{-16} \text{ s}^{-1}$  and the disk half-thickness  $H \sim 300 \text{ pc}$  we find the estimation  $C_\Omega \simeq 100$  which is above the instability excitation threshold. The instability may then produce its own turbulence increasing the diffusivity to the “observed” value of  $\eta_T \sim 10^{26} \text{ cm}^2 \text{ s}^{-1}$ . This picture, if true, has important consequences for the theory of galactic magnetism. In particular, the mean-field theory should be revised to derive the  $\alpha$ -effect and eddy diffusivity for the magnetically excited turbulence. The magnetic field is thus expected to amplify  $\alpha$  and  $\eta_T$  in contrast to the usual concept of magnetic quenching of the turbulent effects.

The alternative approach side-stepping the mean-field formalism was outlined in the Sect. 1. The nonlinear model currently in progress may provide evidence on whether the global nonlinear dynamo-instability in differentially rotating disks is possible.

*Acknowledgements.* This work has been supported in part by the Russian Foundation for Basic Research, project No 96-02-16019.

## Appendix A: the equation system for the global modes

This appendix presents the system of equations governing the global modes of the magnetic shear instability in the differen-

tially rotating disks. The equations are written with the variable  $y$  (18) replacing the axial distance. We drop the subscripts of the vertical,  $l$ , and the azimuthal,  $m$ , wave numbers in the notations for the potential harmonics because the subscripts are everywhere the same in the linear equations. Four dynamical equations of the system include: the equation for the poloidal magnetic field,

$$\begin{aligned} \frac{\partial (\hat{R}A)}{\partial t} &= \left( -g^2 - m^2 \frac{(1-y)^2}{\alpha^2 y^2} \right. \\ &+ \left. \frac{(1-y)^3}{\alpha^2 y} \frac{\partial}{\partial y} y(1-y) \frac{\partial}{\partial y} \right) (\hat{R}A) \\ &- imC_\Omega f(y) (\hat{R}A) - gC_\Omega (\hat{R}\Psi), \end{aligned} \quad (\text{A1})$$

the equation for the toroidal magnetic field,

$$\begin{aligned} \frac{\partial (\hat{R}\mathcal{B})}{\partial t} &= \left( -g^2 - m^2 \frac{(1-y)^2}{\alpha^2 y^2} \right. \\ &+ \left. \frac{(1-y)^3}{\alpha^2 y} \frac{\partial}{\partial y} y(1-y) \frac{\partial}{\partial y} \right) (\hat{R}\mathcal{B}) \\ &- imC_\Omega \hat{R} (f(y)\mathcal{B}) + gC_\Omega (\hat{R}U) \\ &- gC_\Omega \left( f_2(y)(1-y)^2 \frac{\partial A}{\partial y} \right. \\ &+ \left. f_1(y)y^2 \frac{\partial}{\partial y} (1-y)^2 \frac{\partial A}{\partial y} + f_1(y)m^2 A \right), \end{aligned} \quad (\text{A2})$$

the equation for the toroidal flow,

$$\begin{aligned} \frac{\partial (\hat{R}U)}{\partial t} &= \text{Pm} \left( -g^2 - m^2 \frac{(1-y)^2}{\alpha^2 y^2} \right. \\ &+ \left. \frac{(1-y)^3}{\alpha^2 y} \frac{\partial}{\partial y} y(1-y) \frac{\partial}{\partial y} \right) (\hat{R}U) \\ &+ imC_\Omega (f_4(y)U - f(y) (\hat{R}U)) \\ &- gC_\Omega \left( f_4(y)y(1-y) \frac{\partial \Psi}{\partial y} + f_3(y) (\hat{R}\Psi) \right) \\ &- g \frac{\text{Pm Ha}^2}{C_\Omega} (\hat{R}\mathcal{B}), \end{aligned} \quad (\text{A3})$$

and the toroidal vorticity equation,

$$\begin{aligned} \frac{\partial (\hat{R}W)}{\partial t} &= \text{Pm} \left( -g^2 - m^2 \frac{(1-y)^2}{\alpha^2 y^2} \right. \\ &+ \left. \frac{(1-y)^3}{\alpha^2 y} \frac{\partial}{\partial y} y(1-y) \frac{\partial}{\partial y} \right) (\hat{R}W) \\ &- imC_\Omega \hat{R} (f(y)W) + gC_\Omega f_3(y) (\hat{R}U) \\ &+ gC_\Omega f_4(y) \left( y(1-y) \frac{\partial U}{\partial y} + img\Psi \right) \\ &- gC_\Omega \left( f_2(y)(1-y)^2 \frac{\partial U}{\partial y} \right. \\ &+ \left. f_1(y)y^2 \frac{\partial}{\partial y} (1-y)^2 \frac{\partial U}{\partial y} + m^2 f_1(y)U \right) \\ &+ g \frac{\text{Pm Ha}^2}{C_\Omega} (\hat{R}\mathcal{Z}). \end{aligned} \quad (\text{A4})$$

In these equations,  $\alpha = s_0/H$  is the aspect ratio, and  $f$  is the normalized angular velocity (1). Other rotational functions are

$$\begin{aligned} f_1 &= \frac{1}{s} \frac{df(s)}{ds}, \quad f_2 = \frac{1}{s} \frac{d}{ds} s^2 \frac{df(s)}{ds}, \\ f_3 &= \frac{1}{s} \frac{d}{ds} (s^2 f(s)), \quad f_4 = \frac{1}{s} \frac{d}{ds} \frac{1}{s} \frac{d}{ds} (s^2 f(s)), \end{aligned} \quad (\text{A5})$$

The dependence on the vertical wave number,  $l$ , and also the symmetry type of the excitations are involved into the system (A1) - (A4) through the factor  $g$ ,

$$g(l) = \begin{cases} \pi(l-1/2) & \text{for the S-modes} \\ -\pi l & \text{for the A-modes.} \end{cases} \quad (\text{A6})$$

Next two equations relate the toroidal current potential,  $\mathcal{Z}$ , to the poloidal magnetic field and the stream function,  $\Psi$ , to the vorticity function,  $W$ :

$$\begin{aligned} \mathcal{Z} - g^2 A + \frac{1}{\alpha^2} (\hat{R}A) &= 0, \\ W - g^2 \Psi + \frac{1}{\alpha^2} (\hat{R}\Psi) &= 0. \end{aligned} \quad (\text{A7})$$

The above dynamical equations describe the evolution of the potentials affected by the differential operator  $\hat{R}$  (12), not of the potentials themselves. The differential equation,

$$\begin{aligned} (\hat{R}A) + m^2 \frac{(1-y)^2}{y^2} A \\ - \frac{(1-y)^3}{y} \frac{d}{dy} y(1-y) \frac{dA}{dy} = 0, \end{aligned} \quad (\text{A8})$$

should be included into the system to restore  $A$  from the  $(\hat{R}A)$ , and the similar equations are necessary for all other potentials.

The complete system includes twelve joined equations governing the global modes: four dynamical Eqs. (A1) - (A4), two Eqs. (A7) and six Eqs. (A8).

## Appendix B: elementary local analysis

Our numerical results can be interpreted basing on the local stability criteria. This Appendix presents the local analysis for a simple case of an incompressible but diffusive fluid.

We use the Cartesian coordinate system co-rotating with the local angular velocity,  $\Omega_\circ$ , of the fluid at the axial distance  $s_\circ$ . The origin of the reference frame is placed at this distance  $s_\circ$  and the axes  $x, y$  and  $z$  point in the radial, azimuthal, and vertical directions respectively. The local approximation considers excitations with the spatial scales small compared to  $s_\circ$ . Then, the motion in the reference state can be approximated by the shear flow,

$$\mathbf{V}_\circ = e_y \Omega_\circ \beta x, \quad (\text{B1})$$

where  $\beta$  is the normalized shear (7) at the distance  $s_\circ$ . The external vertical uniform magnetic field with the amplitude  $B_0$  is applied.

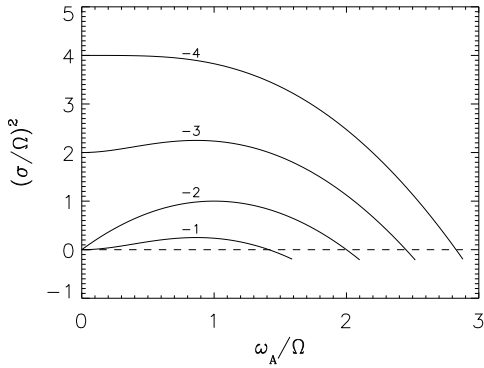


**Fig. 9.** The eigenvalue dependencies on the normalized magnetic field. The lines are marked by the correspondent values of rotational shear  $\beta$  (6)

The linearised MHD equations in the local approximation read (cf. Balbus & Hawley 1991; Brandenburg et al. 1995)

$$\begin{aligned} \frac{\partial \mathbf{V}}{\partial t} - 2\mathbf{V} \times \Omega_o + \Omega_o \beta x \frac{\partial \mathbf{V}}{\partial y} + e_y \Omega_o \beta V_x \\ - \frac{B_0}{4\pi\rho} \frac{\partial \mathbf{B}}{\partial z} + \frac{1}{\rho} \nabla P - \nu \Delta \mathbf{V} = 0, \\ \frac{\partial \mathbf{B}}{\partial t} - B_0 \frac{\partial \mathbf{V}}{\partial z} + \Omega_o \beta x \frac{\partial \mathbf{B}}{\partial y} - e_y \Omega_o \beta B_x - \eta \Delta \mathbf{B} = 0, \\ \text{div } \mathbf{B} = 0, \quad \text{div } \mathbf{V} = 0, \end{aligned} \quad (\text{B2})$$

where  $P$  is the pressure excitation including the magnetic term.

We assume for simplicity that the magnetic Prandtl number equals one,  $\nu = \eta$ , and the excitations do not depend on the horizontal coordinates  $x$  and  $y$ . This later assumption cancels in the Eqs. (B2) the terms with position-dependent coefficients. Then the plane wave solutions,  $\exp(\sigma t + ikz)$ , are possible. The usual condition of zero discriminant gives the dispersion relation,

$$\begin{aligned} (\sigma + \eta k^2)^4 + 2(\sigma + \eta k^2)^2 (\omega_A^2 + \Omega^2(2 + \beta)) + \\ + \omega_A^2 (2\Omega^2\beta + \omega_A^2) = 0, \end{aligned} \quad (\text{B3})$$

where we dropped the subscript “o” of the local angular velocity  $\Omega_o$ ,  $\omega_A = kB_0/\sqrt{4\pi\rho}$  is the Alfvén frequency.

Eq. (B3) has two branches of solutions. One of them is a branch of stable oscillations which are of no interest for this paper. The other branch describes the instabilities:

$$\begin{aligned} (\sigma + \eta k^2)^2 = -\Omega^2(2 + \beta) - \omega_A^2 \\ + \Omega [\Omega^2(2 + \beta)^2 + 4\omega_A^2]^{1/2}. \end{aligned} \quad (\text{B4})$$

When the diffusivity is neglected,  $\sigma^2$  is real. With positive shear,  $\beta \geq 0$ , only negative  $\sigma^2$  exist implying the stable oscillations. If the shear is negative, positive and negative  $\sigma^2$  can be found dependent on the Alfvén frequency.

Fig. 9 shows the plots of  $\sigma^2$  as functions of the magnetic field for several values of the shear. For  $\beta < -2$ , the lines cross the  $\sigma^2$ -axis indicating the nonmagnetic instability. This is

no surprise because Eq. (B4) reproduces the Rayleigh stability criterion,

$$\sigma^2 = \begin{cases} -2\Omega^2(2 + \beta) & \text{for } \beta < -2 \\ 0 & \text{for } \beta \geq -2, \end{cases} \quad (\text{B5})$$

in the limit of zero magnetic field. The branch of solutions of the Eq. (B3) other than (B4) produces stable oscillations (finite negative  $\sigma^2$ ) for  $\beta \geq -2$  in the zero-field limit. Of course, the instability is present for arbitrary amplitude of the magnetic field when the shear is negative,  $\beta < 0$  (Balbus & Hawley 1991; Balbus 1995). With increasing magnetic field the wavelength of the excitations should be proportionally increased to keep the Alfvén frequency in the instability region. With not too strong shear,  $\beta > -4$ , a weak magnetic field produces a destabilising effect:  $\sigma^2$  grows initially with the field amplitude. For  $\beta < -4$ ,  $\sigma^2$  decreases steadily with  $\omega_A$ . When the wave number,  $k$ , is fixed, the system becomes stable for sufficiently strong magnetic field as it should be the case (Chandrasekhar 1961, p.389).

## References

- Balbus S.A., 1995, ApJ 453, 380  
 Balbus S.A., Hawley J.F., 1991, ApJ 376, 214  
 Balbus S.A., Hawley J.F., 1992, ApJ 400, 610  
 Balbus S.A., Hawley J.F., 1994, MNRAS 266, 769  
 Brandenburg A., Nordlund Å., Stein R.F., Torkelsson U., 1995, ApJ 446, 741  
 Brandenburg A., Nordlund Å., Stein R.F., Torkelsson U., 1996, ApJ 458, L45  
 Cowling T.G., 1934, MNRAS 94, 39.  
 Chandrasekhar S., 1960, Proc. Nat. Acad. Sci. 46, 253  
 Chandrasekhar S., 1961, Hydrodynamic and Hydromagnetic Stability. Clarendon, Oxford  
 Curry C., Pudritz R.E., 1995, ApJ 453, 697  
 Curry C., Pudritz R.E., Sutherland P.G., 1994, ApJ 434, 206  
 Deinzer W., Grosser H., Schmitt D., 1993, A&A 273, 405  
 Gammie C.F., Balbus S.A., 1994, MNRAS 270, 138  
 Glatzmaier G.A., 1985, ApJ 291, 300  
 Glatzmaier G.A., Roberts P.H., 1995, Nat 377, 203  
 Hawley J.F., Gammie C.F., Balbus S.A., 1995, ApJ 440, 742  
 Kaisig M., Rüdiger G., Yorke H.W., 1993, A&A 274, 757  
 Kitchatinov L.L., Rüdiger G., 1997, MNRAS, to appear  
 Krause F., Rädler K.-H., 1980, Mean-Field Magnetohydrodynamics and Dynamo Theory. Akademie-Verlag, Berlin  
 Matsumoto R., Tajima T., 1995, ApJ 445, 767  
 Meneguzzi M., Frisch U., Pouquet A., 1981, Phys. Rev. 47, L1061  
 Moffatt H.K., 1978, Magnetic Field Generation in Electrically Conducting Fluid. Cambridge Univ. Press  
 Moss D., Tuominen I., Brandenburg A., 1991, A&A 245, 129  
 Ogilvie G.I., Pringle J.E., 1996, MNRAS 279, 152  
 Pouquet A., Frisch U., Leorat J., 1976, J. Fluid Mech. 77, 321  
 Rüdiger G., Elstner D., Stepinski T.F., 1995, A&A 298, 934  
 Stone J.M., Norman M.L., 1994, ApJ 433, 746  
 Stone J.M., Hawley J.F., Gammie C.F., Balbus S.A., 1996, ApJ 463, 656  
 Tout C.A., Pringle J.E., 1992, MNRAS 259, 604  
 Velikhov E.P., 1959, Sov. Phys. JETP 9, 995  
 This article was processed by the author using Springer-Verlag L<sup>A</sup>T<sub>E</sub>X A&A style file L-AA version 3.